Spirobifluorene Trimers: High Triplet Pure Hydrocarbon Hosts for Highly Efficient Blue Phosphorescent Organic Light-Emitting Diodes

Denis Ari, Yue-Jian Yang, Cassandre Quinton, Zuoquan Jiang, Dong-Ying Zhou, Cyril Poriel

Spirobifluorene Trimers : High Triplet Pure Hydrocarbon Hosts for Highly Efficient Blue Phosphorescent Organic Light-Emitting Diodes.

Denis Ari,[a#] Yue-Jian Yang,[b#] Cassandre Quinton,[a] Zuo-Quan Jiang,[b] Dong-Ying Zhou,[b*] and Cyril Poriel[a*]

a. Univ Rennes, CNRS, ISCR-UMR CNRS 6226, F-35000 Rennes, France- email: cyril.poriel@univ-rennes.fr

b. Institute of Functional Nano & Soft Materials (FUNSOM), Soochow University, 99 Renai Rd., Suzhou Industrial Park Suzhou, Jiangsu 215000. dyzhou@suda.edu.cn

Jiangsu Key Laboratory for Carbon-Based Functional Materials & Devices, Soochow University, Suzhou, Jiangsu 215123, China.

# equal contribution

Abstract

Pure aromatic hydrocarbon materials (PHC) represent a new generation of host materials for phosphorescent OLEDs (PhOLEDs), free of heteroatoms. They reduce the molecular complexity, can be easily synthesized and are an important direction towards robust devices. As heteroatoms can be involved in bonds dissociations in operating OLEDs through *exciton induced degradation process*, developing novel PHCs appear particularly relevant for the future of this technology. In the present work, we report a series of extended PHCs constructed on the assembly of three spirobifluorene fragments. The resulting positional isomers present a high triplet energy level, a wide HOMO/LUMO difference and improved thermal and morphological properties compared to previously reported PHCs. These characteristics are beneficial for the next generation of host materials for PhOLEDs and provide relevant design guidelines. Used as host in blue-emitting PhOLEDs, which are still the weakest link of the field, a very high EQE of 24 % and low threshold voltage of 3.56 V were obtained with a low-efficiency roll-off. This high performance strengthens the position of PHC strategy as an efficient alternative for OLED technology and opens the way to a more simple electronic.

Keywords: Phosphorescent Organic Light-Emitting Diodes, Blue Emission, Organic Electronics, Spirobifluorene, Pure Aromatic Hydrocarbons, Host Materials.

Introduction

Organic Electronic technology has started to change our daily life with notably the development of Organic Light-Emitting Diodes (OLEDs) technologies.[1] For the last 25 years, phosphorescent OLEDs (PhOLEDs), the second generation of OLEDs,[2-5] have been the subject of intense researches, which have allowed to release this generation of OLEDs on the market. In this field, blue emission is particularly challenging and blue PhOLEDs have always been the weakest link of this technology,[6-9] notably due to their low stability, which has hindered their commercialization. The Emissive Layer (EML) of a PhOLED is constituted by the combination of a phosphorescent emitter and a host

material. By a cascade of energy transfers, 100% of the excitons can be recovered.[10, 11] Thus, the host has a crucial role in the final device performance and the development of high-efficiency hosts has concentrated a fantastic attention since the discovery of PhOLEDs in 1998.[2] The molecular design of host materials has even been a driving force in this field.[3-5, 7, 12-15] Nowadays, the design characteristics are well known and an ideal host for a blue PhOLED should present several key properties: i) a high triplet energy (E_{T1}>2.8 eV) to confine excitons into the emitter in order to avoid back energy transfers, (ii) a large HOMO/LUMO gap to promote charge recombination into the emitter, (iii) high thermal and morphological stabilities for device lifetime and (iv) robust chemical bonds, which cannot be easily broken by the energy of excitons formed for blue emission. This last point has been particularly studied in the last years and it has been shown that C–N, C–P and C–S bonds, widely found in the molecular backbone of almost all the very high efficiency host materials reported to date, can be broken by the high energy of blue excitons (ca 3 eV).[16-19] The key role played by the bond dissociation energies in OLEDs degradation has been reported in 2013 and is named *exciton induced degradation process*.[20] The importance of bond dissociation energies has also been revealed by the group of Bredas, in 2019, showing that the phosphorus-carbon bonds of aryl phosphoryl units can be more easily dissociated in their T_1 states than in their ground (S_0) states.[19] Pure hydrocarbons (PHC) host materials, which are molecules free of heteroatoms, have thus emerged as a solution for the next generation of blue PhOLEDs. Despite initially reported in 2005,[21] the performance of PHC as host for red, green or blue phosphors (the first example of PHC in a blue PhOLED was reported by Liu and coworkers in 2009[22]) is stayed modest during many years[23-27] until several reports have started to show that very high performances can be reached as for their heteroatom-based counterparts.[28-33] PHCs now appear as a credible solution to heteroatoms-based hosts.[34, 35] This new generation of hosts also has the advantages of molecular simplicity and simple large-scale synthesis and can be therefore reasonably seen as key actors for the future. However, the number of high performance blue PhOLEDs using a PHC is still weak[29] and there is a room for improvement in term of molecular designs as the molecular diversity of current PHCs is very poor. In this context, improving the physical properties keeping in the meantime all the other properties unaltered (high E_{T1} and wide HOMO/LUMO gap) appear for example as an important goal for the future in order to continue to improve the OLED technology.

In this work, we report a series of novel PHC hosts constructed on the molecular assembly of three SpiroBiFluorene (**SBF**) units. In order to maintain a high E_{T1} and a wide HOMO/LUMO energy gap, the design strategy is based on the electronic disruption of the π−conjugation of the three **SBF** fragments. Three positional isomers of SBF-based trimers have been considered: **Trim-C1**, **Trim-C3** and **Trim-C4**. Using positional isomerism to design functional materials is nowadays an efficient strategy to finely tune their electronic properties for a desired application.[36-39] Due to the presence of the three **SBF** units, known to be one of the most appealing building block to reach morphologically stable materials,[40-44] the present trimers should possess, in principle, improved thermal properties keeping nevertheless the electronic properties of the **SBF** monomer unaltered (high E_{T1}/E_{S1}, large HOMO/LUMO gap). The three trimers investigated herein are built on a central **SBF** substituted at C3 and C6 positions. These positions of substitutions form a *meta* linkage with the central bridged biphenyl core, which should have a significant impact on the π-conjugation disruption with the two pending SBF units, avoiding in turn a drop of both E_{T1} and E_{S1}. Given that the substitution of these external **SBF** units is also important in the device performance, three different patterns will be investigated, all significantly disrupting the π-conjugation as well. All these trimers successfully achieve a high $E_{T1}/E_{S1,}$ wide HOMO/LUMO gap and excellent thermal/morphological properties with very high decomposition and glass transition temperatures (T*d* and T*g*). These properties are significantly improved compared to the other PHCs reported to date. Incorporated as host in blue PhOLEDs using FIrpic (bis[2-(4,6-difluorophenyl)pyridinato-C2,N](picolinato)iridium(III)) as emitter, **Trim-C1** displays a very high performance with an External Quantum Efficiency (EQE) of 24% and a very low threshold voltage V_{on} of 3.56 V. **Trim-C4** also presents high performance with

EQE/V_{on} of 20.5% / 3.56 V. These high performance show the relevance of the molecular approach and the strong potential of PHCs as host in blue-emitting PhOLEDs.

Results and discussion

The synthetic approach proposed is first based on the synthesis of the key platform **3,6-diBr-SBF**, synthesized from corresponding 3,6-dibromofluorenone and iodobiphenyl (nucleophilic addition followed by intramolecular aromatic electrophilic substitution of the fluorenol). **Trim-C3** and **Trim-C4** were then further obtained with high yields at the gram scale from classical Suzuki-Myaura cross coupling with the corresponding pinacol derivative, either **3-Bpin-SBF** or **4-Bpin-SBF** (72 and 70% *resp.*). Surprisingly, this approach was unsuccessful with the C1 isomer maybe due to the high steric congestion induced by the C1 position. The synthesis was then performed by first synthesizing the dipinacol analogue **3,6-diBPin-SBF** further coupled to the **1-Br-SBF** with a yield of 65%. These approaches were extremely simple and efficient at the gram scale, which are key points nowadays in material science.

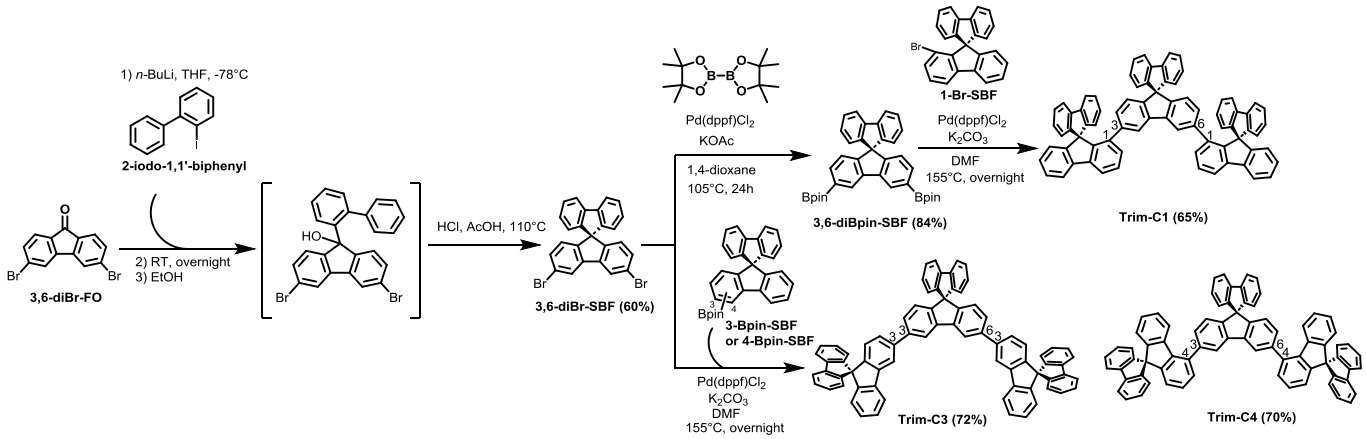

Figure 1. Synthesis **Trim-C1**, **Trim-C3** and **Trim-C4**

The molecular construction of the SBF isomers is at the origin of the electronic properties discussed below. As the three isomers are constructed on the same 3,6-SBF scaffold, the different electronic properties can only be imputed to the substitution pattern, C1, C3 or C4, of the external SBFs. The 3,6-SBF platform has been chosen as the C3 and C6 position form a *meta* linkage with the central biphenyl linkage, which should reduce the electronic coupling between the SBF fragments. This is a different behaviour to the well-known 2,7-SBF platform, widely developed in literature,[40-42] which increases the π-conjugation pathway. The external SBFs attached display a different substitution pattern, either C1 (in **Trim-C1**), C3 (in **Trim-C3**) or C4 (in **Trim-C4**). These three positions are supposed to restrict the electronic coupling of the external SBFs with the central one due to a combination of *meta* linkages and/or steric hindrance. These characteristics are the fundations of the present design in order to fit with an application as host material for a blue PhOLED.

The three isomers display different UV-visible absorption profiles, which highlight the importance of the substitution pattern on the π-conjugation disruption (Figure 2, Top-Left). First, it should be noted that the three isomers present a main band between 308 and 310 nm, characteristic of the SBF scaffold. The intensity of the electronic coupling between the three SBFs can be evaluated by the contribution observed at higher wavelengths. This contribution is different for each isomer. Indeed, for **Trim-C3**, this band is intense and translates an extension of the π-conjugation compare to the two other trimers., This band is significantly decreased in **Trim-C4** and is even not dectected in **Trim-C1**. However, TD-DFT studies (Figure S42-S44, Table S5-7) indicate that this band also exists in **Trim-C1** but is blue shifted and of low intensity. Thus, despite larger, the absorption profile of **Trim-C1** is the most similar to that of **SBF** monomer,[36] showing that the two SBF units attached at C1 less influence the absorption properties than in the two other isomers. This shows that the C1 site

efficiently breaks the conjugation between the three SBF units, which will have important consequences on the triplet state energy level discussed below. This feature is caused by the joint effect of a strong steric hindrance and a *meta* biphenyl linkage. Oppositely, the two other trimers, **Trim-C4** and **Trim-C3**, only provide partial conjugation breaking, in accordance with structurally related systems.[36] Nevertheless, for **Trim-C1**, the band at 310 remains larger than for **SBF**, translating that the π–conjugation disruption is not complete. TD-DFT calculations and natural transition orbital (NTO) representations show that the main band is due to transitions localized on isolated fluorene parts for the three trimers (Figure S42-S44). The band at lower energy experimentally found at around 319 nm is modelized in the case of **Trim-C3** by two transitions displaying a wavelength shift of 10 and 16 nm compared to the transitions responsible of the main band (experimentally found at 309 nm), in agreement with what can be experimentally observed. The NTOs involved in the two low energy transitions are localized on the substituted fluorene of the central SBF on the one hand and on the three adjacent fluorenes on the other hand. In the case of **Trim-C4**, the transitions responsible for the band at low energy are theoretically shifted by 9 and 12 nm (shoulder experimentally at around 317 nm) compared to the transitions of the main band (experimentally found at 308 nm). As for **Trim-C3**, the NTOs of **Trim-C4** implied in the low energy transitions responsible of the shoulder are localized on the substituted fluorene of the central SBF on the one hand and on the three adjacent fluorenes on the other hand. Due to the high dihedral angles between the adjacent fluorenes in **Trim-C4** compared to **Trim-C3** (59 *vs* 39°, see Figure S46) and the difference in term of linkage (*ortho* linkage for **Trim-C4** and *meta* linkage for **Trim-C3**), the conjugation and thus the wavelength is reduced in accordance with the experimental data. Note that the calculated oscillator strengths of the transitions responsible for the low energy band in **Trim-C4** are also lower than that in **Trim-C3** (0.55 and 0.19 vs 0.61 and 0.20). Transitions corresponding to a low energy band are also modelized in the case of **Trim-C1**, however with a small wavelength shift of 2 and 8 nm compared to the transitions of the main band. The low energy band is experimentally partially hidden by the main band. This is the reason why we the experimental spectrum of **Trim-C1** is larger than that of **SBF** but does not show any distinct band at low energy such as that of **Trim-C3** and **Trim-C4**. Moreover, the C1 substitution avoids the delocalization on the three adjacent fluorenes and the NTOs implied in the lowest energy transitions are localized on the substituted fluorene of the central SBF on the one hand and on the external SBFs on the other hand. Therefore, the theoretical data are in good agreement with the experimental absorption spectra. The optical gaps (ΔE_{opt}, determined from the onset of the absorption spectra in cyclohexane) also reflect these different π-conjugation breaking as a contraction is observed from **Trim-C1** (3.81 eV), **Trim-C4** (3.73 eV) and **Trim-C3** (3.66 eV). They are all significantly contracted compared to that of **SBF** (3.97 eV) in accordance with the above mentionned conclusions. These gaps are compatible with a use as hosts in blue PhOLEDs as detailed below.

The substitution pattern also strongly affects the emission properties (Figure 2, Top-middle). **Trim-C1** displays the most blue shifted spectrum (λ_{max} = 325 nm), only slightly red shifted compare to that of **SBF** monomer, (λ_{max} = 310 and 323 nm, Figure 2, Table 1) and in accordance with its very large ΔE_{opt} as exposed above. The steric hindrance induced by the C1 position hinders the planarization at the excited state as shown by theoretical calculations, Figure S46-47. This leads to a greater number of emitting conformers in accordance with an unresolved spectrum. **Trim-C3** presents a very different spectrum, well-structured and red shifted in accordance with a planarization at the excited state (λ_{max} = 345 nm). The Stokes shift is thus increased. The planarization is confirmed by theoretical calculations, which reveal that the dihedral angle between two SBFs is significantly decreased from 39° in S_0 to 16° in S_1 in **Trim-C3**, Figure S46. The C/C bond linking the two fluorenes is also decreased (Figure S48). This is the consequence of a relaxed environment, different from what is observed for the C1 isomer. **Trim-C4** is again different as its emission spectrum is significantly red shifted by 40 nm compared **Trim-C1** (λ_{max} = 365 nm) with a large Stokes shift. As observed for **Trim-C3,** the dihedral angle of **Trim-C4** decreases from S_0 to S_1 states but remains at ca 30° due to the constrained environment. It should be mentioned that the fluorescence of C4-SBF derivatives has been the subject of several studies but has not been fully unravelled to date.[42, 45, 46] Interestingly, the quantum yields of these trimers are high from 0.82 for **Trim-C3**, 0.65 **Trim-C4** and 0.56 for **Trim-C1** due to the presence of three adjacent SBF units. The higher value observed for **Trim-C3** can be assigned to the low non-

radiative constant k_{nr}, which is weak compared to the high radiative constant k_r (0.043 and 0.195 ns^{-1} respectively). For both **Trim-C3** and **Trim-C4**, the high k_r can be related to the high oscillator strength observed for the low energy transition. It is also interesting to note that the constrained environment found in **Trim-C4** and **Trim-C1** increases their k_{nr} (0.131 and 0.098 ns^{-1} respectively), whereas that of **Trim-C3** (0.043 ns^{-1}) is significantly shorter due to its relaxed linkage. Therefore, these materials appear to be versatile as they will be used herein as hosts for PhOLED but they could also be used as emitter in OLED.

It is interesting to mention that compared to their dimer analogues (with identical substitution patterns), previously reported in literature,[36] the present trimers display similar absorption and emission spectra with only a slight shift (below 5 nm). This indicates that the additional SBF fragment only has a limited influence on the absorption/emission maxima due to the restricted conjugation pathways and shows the efficiency of the design strategy.

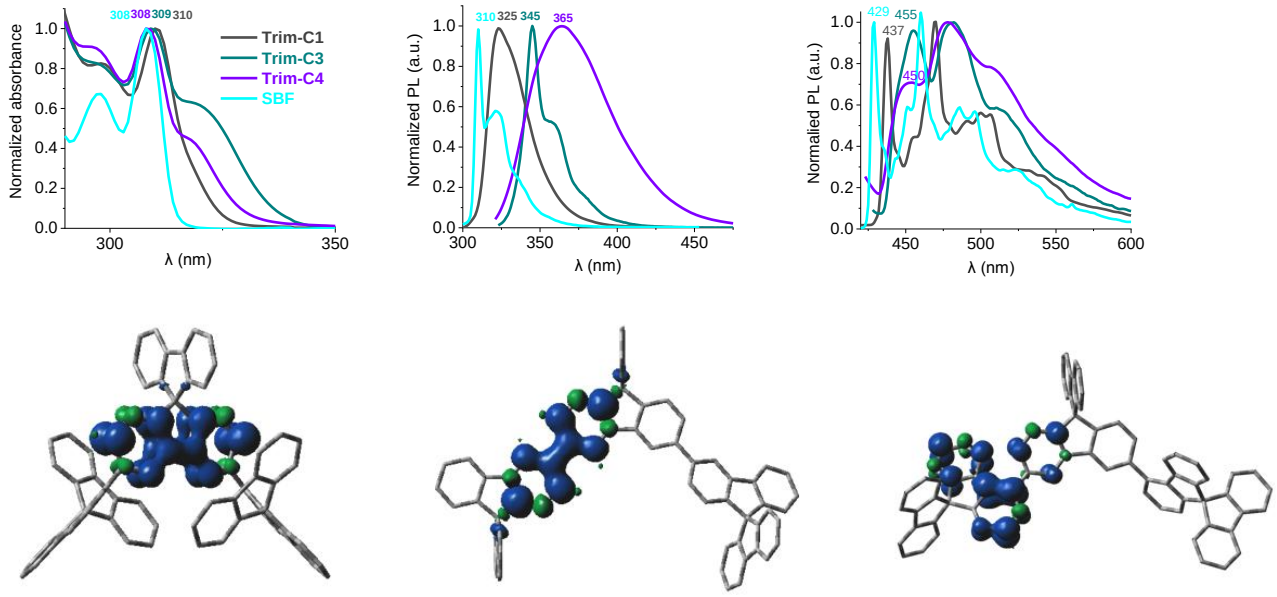

Figure 2. Top. Normalized experimental absorption (left, in cyclohexane), emission at room temperature (middle, in cyclohexane) and emission at 77 K (right, in 2-Me-THF) spectra of **Trim-C1** (grey lines), **Trim-C3** (green lines) and **Trim-C4** (violet lines). **SBF** (cyan lines) has been added for comparison. Bottom. Spin density distribution (SDD) of the triplet of **Trim-C1**, **Trim-C3** and **Trim-C4** (isovalue = 0.004).

The emission spectra measured at 77 K in 2-MeTHF (Figure 2, Top-right) provide the corresponding E_{T1} of **Trim-C1** (2.84 eV, λ=437 nm), **Trim-C4** (2.75 eV, λ=450 nm) and **Trim-C3** (2.73 eV, λ=455 nm). The highest E_{T1} was then obtained with **Trim-C1**, which possesses, in the light of absorption studies, the most efficient π-conjugation disruption. This E_{T1} is very high and close to that of unsubstituted **SBF** (2.89 eV, λ=429 nm), showing the relevance of the present design. The trend observed in absorption is also followed for the two other trimers. Indeed, the E_{T1} of **Trim-C4** (2.75 eV) is slightly higher than that of **Trim-C3** (2.73 eV), translating different degree of π-conjugation disruption. Thus, despite different E_{S1}, these two trimers possess similar E_{T1}, which represent an interesting degree of excited states tuning. For the three compounds, the E_{T1} is maintained high, which is a key property to insure efficient energy transfer with the blue emitting phosphor in the OLED. The difference between the three isomers can be rationalized by the spin density, which is exclusively localized on one fluorene for **Trim-C1**, whereas delocalization is observed for **Trim-C4** and **Trim-C3** (Figure 2, bottom). The trend obtained experimentally is also well reproduced by theoretical calculations (2.57, 2.47 and 2.46 eV, see Table S8). Finally, these T_1 states present a very long lifetime, evaluated between 6.5 and 4.1 s (Table 1). To sum up, the three trimers display a high E_{T1} and E_{S1}, which can be modulated, in a different extend, by the substitution pattern. The most efficient

π-conjugation disruption is detected for **Trim-C1** due to its C1 position leading to the highest E_{S1} and E_{T1}.

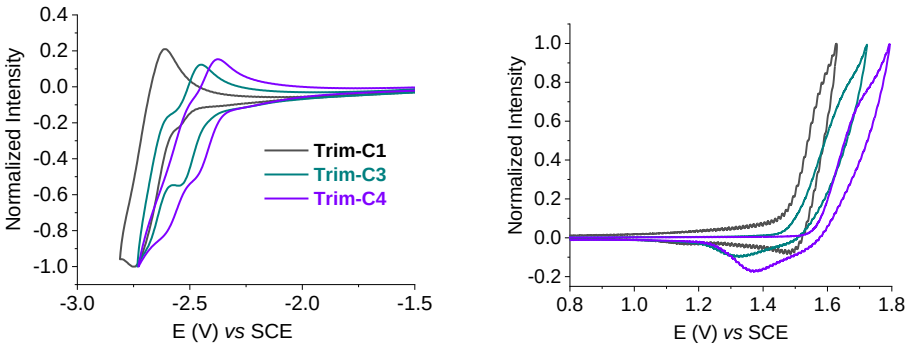

Figure 3. **Trim-C1** (grey lines), **Trim-C3** (green lines) and **Trim-C4** (violet lines). Cyclic voltammetry data (left: in reduction: DMF/[NBu_4PF_6] 0.1 M, right: in oxidation: CH_2Cl_2/[Bu_4NPF_6] 0.2 M; sweep rate of 100 mV^{-1}, platinum disk working electrode).

Electrochemical investigations were performed thanks to cyclic voltammetry (CV) in DMF (reduction, Figure 3, left) and CH_2Cl_2 (oxidation, Figure 3, right) in order to evaluate the HOMO and LUMO energy levels respectively.

The HOMO levels were measured at -5.88 eV for **Trim-C1**, at -5.90 eV for **Trim-C3** and at -5.97 eV for **Trim-C4**, these values being close to that of **SBF** (-5.97 eV). Thus, despite the presence of three connected SBF units, **Trim-C4** displays a very deep HOMO energy identical to that of **SBF** monomer, the effect arising from the trimerization (the HOMO should increase) being almost entirely erased. This is what we expect for the present molecular design strategy. The cases of **Trim-C1** and **Trim-C3**, which display similar HOMO energy levels both higher than that of **Trim-C4**, appear more surprising in the light of previous works on structurally related compounds.[36] This will be discussed below after detailing the LUMO evolution. The cathodic studies reveal for all compounds a reduction wave at a low potential below -2.4 V, providing LUMO energy levels evaluated at -1.83 eV for **Trim-C1**, at -1.98 eV for **Trim-C3** and at -2.06 eV for **Trim-C4**. This time only the value measured for **Trim-C1** is similar to that of **SBF**. The different evolution than that exposed above for the HOMO energy levels can be understood considering the nature of the phenyl linkages (*ortho vs meta*) and the steric hindrance (the dihedral angle between the SBF units), which are the two main parameters involved in the electronic properties. This has been discussed elsewhere.[36] The main finding was linked to the different impact these parameters have on the benzenoidal HOMO or on the quinoidal LUMO. The torsions (steric effect) have a larger influence on the HOMO energy than on the LUMO energy, whereas the linkages (*ortho*, *meta* and *para*) have a strong influence on the LUMO energy. The trimers studied herein also follow these evolution rules. The LUMO energy of **Trim-C4** with its *ortho* linkage is thus lower in energy than those of **Trim-C1** and **Trim-C3**, which possess a *meta* linkage. The difference between **Trim-C1** and **Trim-C3** both possessing a *meta* linkage is therefore assigned to the more sterically hindered environment of the former inducing a higher LUMO energy level.

For the HOMO, the high steric hindrance found in **Trim-C4**, due to its linkage, induces a lower HOMO energy compare to that **Trim-C3**, with its non-sterically hindered environment. **Trim-C1** appears in this case a peculiar example as its HOMO is the highest in the series despite high fluorene/fluorene dihedral angle (between 62 and 78°, see Figure S51). This can be assigned to the particular molecular arrangement of **Trim-C1**, which favours strong intramolecular interactions between the central terfluorene core and cofacial fluorene units. Indeed, several very short intramolecular carbon/carbon distances (shorter than the sum of the van der Waals radii, 3.4 Å) have been measured indicating significant π–π interactions (Figure S52-S54). This feature is also confirmed by the electrostatic potential surface obtained by molecular modelling, which clearly shows intramolecular interactions, which are absent from the two other trimers **Trim-C3** and **Trim-C4**

(Figure S45). As such π–π interactions are known to increase the HOMO energy level,[47-49] **Trim-C1** displays then a higher HOMO energy than its isomer **Trim-C3** and does not follow the rules previously reported in the literature.[36] The HOMO-LUMO gap (ΔE_{el}) of all the molecules are wide, 3.92 eV for **Trim-C3**, 3.91 eV for **Trim-C4** and 4.05 for **Trim-C1**, which is essential to nest the phosphorescent complex in the emissive layer of the device (see below). One can nevertheless note a gap contraction compared to that of **SBF** (4.16 eV) by selectively reducing the LUMO level energy.

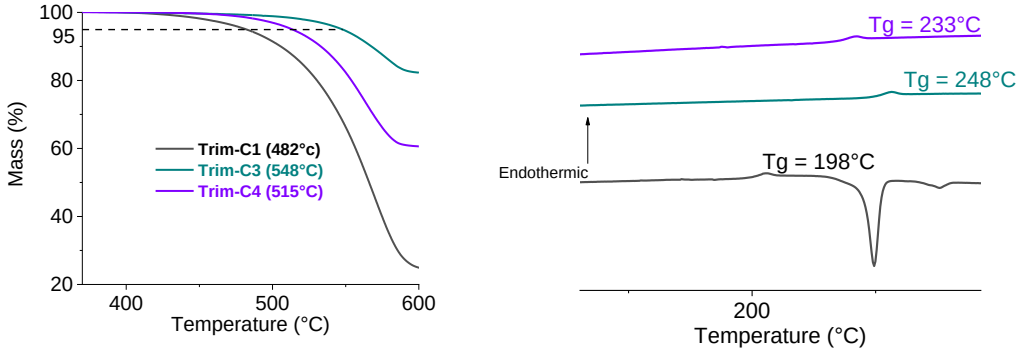

Figure 4. TGA (Left) and DSC (Right) traces of **Trim-C1** (grey lines), **Trim-C3** (green lines) and **Trim-C4** (violet lines).

The thermal and morphological properties of the three trimers have been further investigated by thermogravimetric analysis (TGA) and differential scanning calorimetry (DSC) and have highlighted their excellent stability, a key feature in the present approach. The decomposition temperatures (T_d), measured at 5 % mass loss, of **Trim-C1**, **Trim-C3** and **Trim-C4** are recorded very high at 482, 548 and 515 °C, respectively. In addition, the glass transition temperatures T_g are also very high, above 200°C (205°C for **Trim-C1**, 256°C for **Trim-C3** and 241°C for **Trim-C4**), which is rarely observed for host materials as the molecules used for that purpose are usually of small size to keep a high E_{T1}. The different molecular arrangements of the three trimers are surely the reason of the different Tg. There is an important difference between both **TRIM-C3** and **TRIM-C4** on one side and **TRIM-C1** on the other side. Indeed, in **TRIM-C1**, such as in many C1-based fluorenes, previously reported in literature,[50, 51] π–π interactions are detected (see Figure S45). In Trim-C1, the interactions involve the central terfluorene core and the cofacial fluorene units. This structural feature can be at the origin of the different T*g* observed herein. It should also be mentioned that the T*d* is also measured lower for **TRIM-C1** *vs* both **TRIM-C3** and **TRIM-C4**. In literature, such a difference in term of thermal properties has been previously observed for positional isomers of SBF-liked compounds.[52] Thus, the present T_d and T_g of the trimers are significantly higher than those recently reported for their dimers counterparts[53, 54] or other very high efficiency SBF-based PHC hosts.[28, 30] This shows the efficiency of the present design strategy based on trimers.

Table 1. Selected properties of **Trim-C1**, **Trim-C3** and **Trim-C4**, for **SBF** is used comparison[30]

	Trim-C1	**Trim-C3**	**Trim-C4**	**SBF** [30]
λ_{abs} [nm][a]	310	309	308	308
λ_{em} [nm][a]	325	345	365	310
QY	0.56[b]	0.82[b]	0.65[b]	0.55[c]
$\lambda_{phopsho}$ [nm][d]	437	455	450	429
τ_f [ns][a]	4.5	4.2	2.7	4.6
k_r ($x10^7$) [s^{-1}]	12.5	19.5	24.3	12
k_{nr} ($x10^7$) [s^{-1}]	9.8	4.3	13.1	10
$\tau_{p\ (s)}$	6.5	4.9	4.1	5.4
E_{S1} [eV][e]	4.01	3.76	3.81	4.05
E_{T1} [eV][f]	2.84	2.73	2.75	2.89
LUMO $_{El}$ [eV][g]	-1.83	-1.98	-2.06	-1.81
LUMO $_{th}$ [eV]	-1.37	-1.40	-1.33	-1.26
HOMO $_{El}$ [eV][h]	-5.88	-5.90	-5.97	-5.97
HOMO $_{th}$ [eV]	-5.81	-5.79	-5.84	-5.99
ΔE_{el} (eV)	4.05	3.92	3.91	4.16
ΔE_{th} (eV)	4.44	4.39	4.51	4.73
ΔE_{opt} (eV)[i]	3.81	3.66	3.73	3.97
Tg [°C]	198	248	233	—
Td [°C]	482	548	515	234
μ_h ($x10^{-8}$) [$cm^2.V^{-1}.s^{-1}$][j]	8.41	0.343	1.06	—
μ_e ($x10^{-8}$) [$cm^2.V^{-1}.s^{-1}$][k]	0.225	0.506	1.27	—

[a] In cyclohexane. [b] Compared to SBF. [c] Compared to quinine sulfate. [d] in 2-methyl-THF at 77 K. [e] Calculated from the onset of the lowest energy band in cyclohexane (1239.84/λ). [f] Calculated from the peak maximum of the highest energy phosphorescent band, (1239.84/λ), at 77 K in 2-MeTHF. [g] from CVs in DMF. [h] From CVs in DCM. [i] Calculated from the onset of the UV/Vis absorption spectrum in cyclohexane. [j] Hole mobility. [k] Electron mobility. th = theoretical, El = electrochemical, opt = optical.

Hole-only and electron-only devices (HODs and EODs) were further investigated to measure the charge mobilities (Figure S55). Under low bias, the curves were fitted in the space-charge-limited current (SCLC) region. The three trimers present low mobilities, μ_E=2.25×10^{-9}/μ_H=8.41×10^{-8} cm^2 V^{-1} s^{-1} for **Trim-C1**, μ_E=5.06×10^{-9}/ μ_H=3.43×10^{-9} cm^2 V^{-1} s^{-1} for **Trim-C3** and μ_E=1.27×10^{-8}/ μ_H=1.06×10^{-8} cm^2 V^{-1} s^{-1} for **Trim-C4**. Interestingly, despite these low mobilities, one can note that the charge balance is well equilibrated. Given that ambipolarity (similar hole and electronic mobilities) is a crucial consideration in OLEDs for achieving high performance,[31, 55, 56] the current materials seem particularly intriguing. Like other PHC systems previously reported in the literature, which also exhibit similar hole and electron mobilities,[30, 34] it can be concluded that this is a specificity of PHCs. This appears particularly interesting for further designs as this characteristic is more difficult to reach with heteroatom-based hosts, due to the intrinsic nature of the constituting functional units, which can be strongly electron-rich or strongly electron-poor.

Finally, the trimers were incorporated as hosts for blue PhOLEDs. The Iridium complex FIrpic was used as phosphorescent emitter.[57, 58] The PhOLEDs architectures are: ITO/ HAT-CN (10 nm)/ TAPC (40 nm)/ TCTA (10 nm)/ mCP (10 nm)/ host: FIrpic (15 wt%, 20 nm)/ TmPyPB (40 nm)/ Liq (2 nm)/ Al (120 nm). The energy level diagrams and molecular structures of the above materials are shown in Figure S56. HAT-CN/ Liq are used as hole/electron-injecting layer, TAPC/ TmPyPB as hole/electron-transporting layer and TCTA and mCP as exciton-blocking layers. As HOMO/LUMO of FIrpic (-5.8 eV/-3.1 eV)[55] are nested within those of the three trimers, the charge are injected and carried by the emitter.

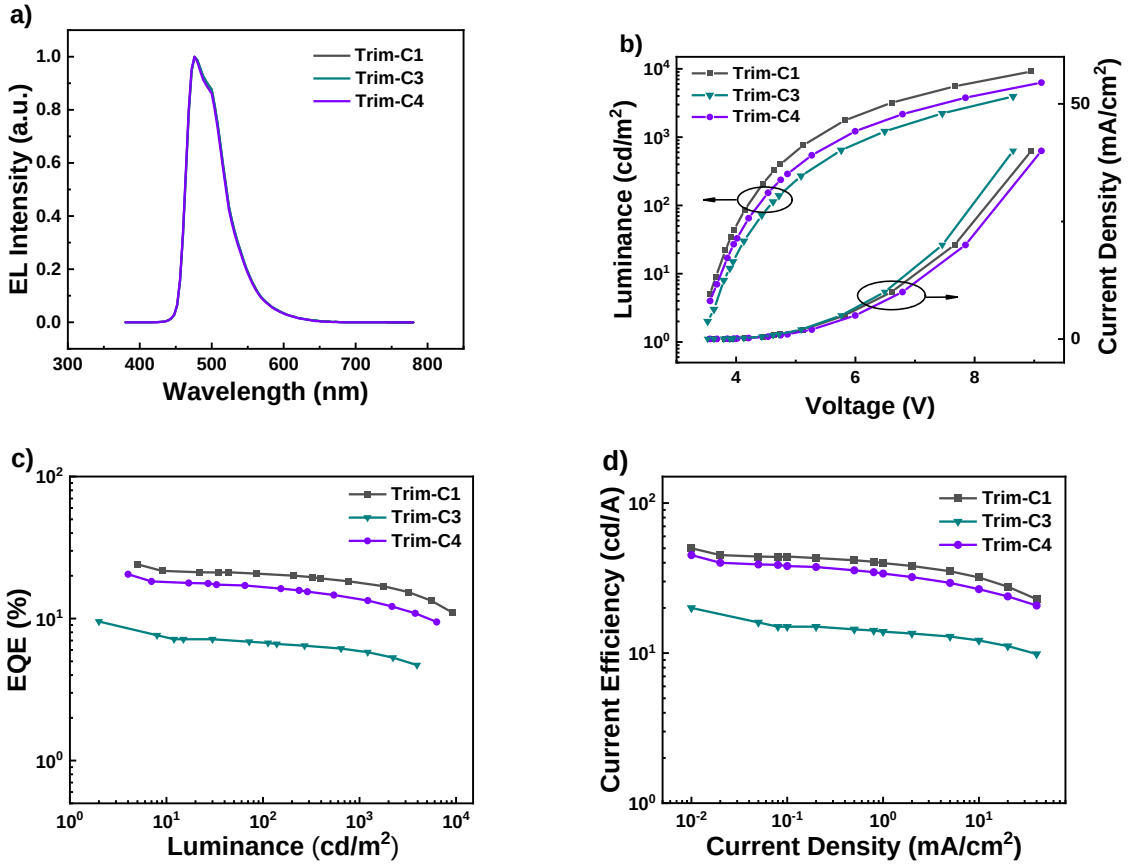

Figure 5. EL spectra (at 5 mA/cm^2) and device performance of blue PhOLEDs (a-d) using **Trim-C1, Trim-C3** and **Trim-C4** as host, respectively. ITO/ HAT-CN (10 nm)/ TAPC (40 nm)/ TCTA (10 nm)/ mCP (10 nm)/ host: FIrpic (15 wt%, 20 nm)/ TmPyPB (40 nm)/ Liq (2 nm)/ Al (120 nm)

The device performances are summarized in Table 2 and Figure 5. For all devices, a blue-light emission at 476 nm with almost identical Commission Internationale de l'Éclairage (CIE) coordinates of (0.15, 0.37/0.38) is measured, indicating independence of the emission from the host materials. The threshold voltages (V_{on}) are very low, at 3.5/3.6 V, indicating efficient charge injection in all the trimers. **Trim-C1** exhibits an exceptionally high external quantum efficiency with a peak value (EQE) of 24.1%. The corresponding maximum current efficiency (CE) and maximum power efficiency (PE) were also very high as measured at 50 cd/A and 44.1 lm/W. Furthermore, **Trim-C4** also displays a very high EQE of 20.5% with CE and PE measured at 45 cd/A and 40.3 lm/W. As the current density increases, it is observed that **Trim-C1** exhibits greater stability than **Trim-C4**, maintaining an EQE of 17.9% at 1000 cd/m^2, demonstrating a low-efficiency roll-off. Surprisingly, the performance of **Trim-C3**, which displays very similar properties at the molecular level, appear to be particularly low. This shows the difficulty to rationally design host materials for high-performance PhOLED. To shed light on the different performance in this series, the quantum yield of the different EML (15 wt% of FIrpic) were measured. The EMLs of 10 wt% FIrpic doped into **Trim-C1**, **Trim-C3** and **Trim-C4** show quantum yields of 0.82, 0.21 and 0.52 respectively. Thus, one can note that the quantum yield of the EML using **Trim-C1**, 0.82, is considerably higher compared to others in accordance with the device performance obtained. In addition, it can be hypothesized that the twisted structure of **Trim-C1** plays a crucial role in providing a more pronounced horizontal orientation to the EML, consequently enhancing the efficiency of the device. Subsequently, we fabricated films by incorporating 15 wt% of FIrpic into the three hosts and assessed the horizontal dipole ratios (Figure 7). These experiments reveal that films derived from **Trim-C1** indeed exhibit a preferential horizontal orientation, with a ratio of 88%. This finding could potentially elucidate the notable efficiency improvement observed in devices based on **Trim-C1** when compared to the other two devices.

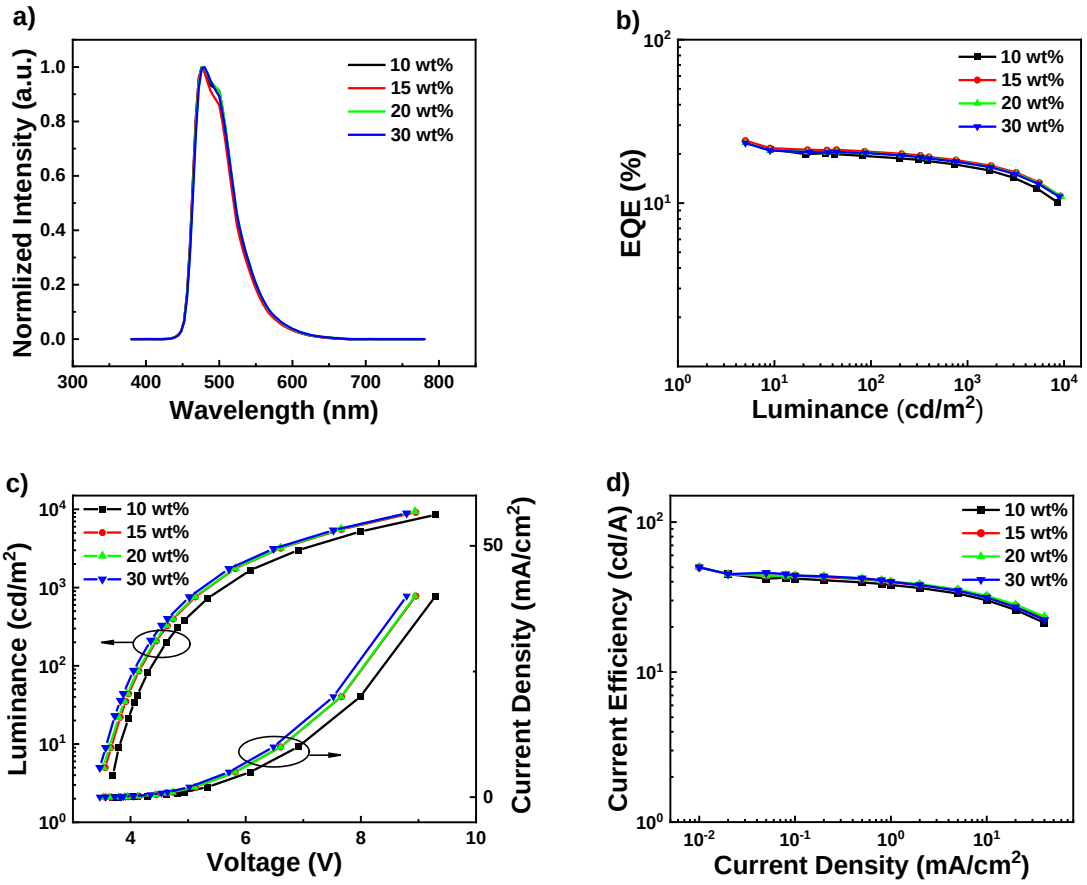

Figure 6. EL spectra (at 5 mA/cm^2) and device performance of blue PhOLEDs (a-d) using **Trim-C1,** at different doping concentrations, respectively. ITO/ HAT-CN (10 nm)/ TAPC (40 nm)/ TCTA (10 nm)/ mCP (10 nm)/ host: FIrpic (10 to 30 wt%, 20 nm)/ TmPyPB (40 nm)/ Liq (2 nm)/ Al (120 nm)

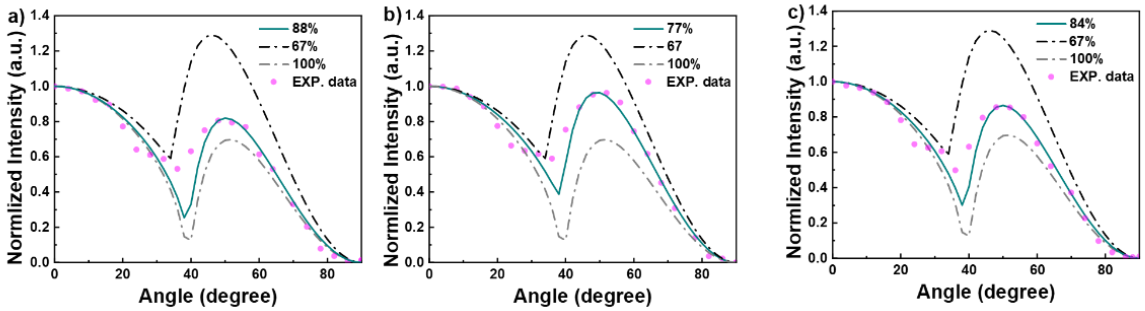

Figure 7. Angle-dependent p-polarized photoluminescence intensity and simulation curve for FIrpic in a) **Trim-C1**, b) **TRIM-C3** and c) **TRIM-C4** films with 15 wt% doping concentration.'

Table 2. Summary of devices performance (15% FIrpic)

	V_{on} [a] (V)	CE[b] (cd/A)	PE[b] (lm/W)	EQE[c] (%)	λ_{max} [d] (nm)	CIE (x,y) [d]
Trim-C1	3.56	50	44.1	24.1/20.6/17.9	476	(0.15, 0.38)

Trim-C3	3.52	20	17.8	9.6/6.8/5.9	476	(0.15, 0.38)
Trim-C4	3.56	45	40.3	20.5/16.7/13.7	476	(0.15, 0.37)

[a] The operating voltage at onset. [b] Values of CE, and PE at the maximum. [c] Values of EQE at the maximum, 100 cd m^{-2} and 1000 cd m^{-2}. [d] Measured at a driving current density of 5 mA cm^{-2}.

As the charges are injected and carried by the dopant, the amount of phosphorescent emitter has been increased in order to determine its impact on the device performance. With the elevated doping concentration of FIrpic, the device's performance, utilizing **Trim-C1** as the host, exhibited negligible variations. Even at a substantial doping level of 30% FIrpic, it consistently maintains a high EQE of 23.3%, as depicted in Figure 6 (the device performances are gathered in Table S18). This suggests that the host material **Trim-C1** can very well dispersed the guest material FIrpic in the emissive layer, suppressing the concentration quenching of FIrpic, thereby avoiding triplet–triplet annihilation (TTA) and triplet–polaron annihilation (TPA).

Conclusions

In summary, we report herein a series of high performance PHC hosts for blue PhOLED applications. With their simple structures, only based on the association of benzene units, PHCs have appeared in recent years as very appealing materials for PhOLEDs. The design discussed in this work, based on the assembly of three SBF units displaying different π-conjugation breaking points, allows to reach high E_{T1}/E_{S1}, wide HOMO/LUMO gap and very high T*d* and T*g*. This last characteristic is of key importance for industrial applications and represents herein a significant improvement compare to the other PHCs reported to date. This consituted, in term of molecular design, a real progress and shows that the oligomerization with judicious substitution pattern constitutes a promising strategy to reach very high performance and stable materials. The charge carrier mobilities, despite very low, appear to be well balanced, which is an important feature in OLED technology. Incorporated as host in blue PhOLEDs using FIrpic as emitter, both **Trim-C1** and **Trim-C4** present a very high EQE and a low V_{on} of 24.1% / 3.56 V and 20.5% / 3.56 V respectively. As these materials can be easily and efficiently synthesized, this work shows that the PHC design strategy is relevant for the next generation of hosts.

Acknowledgment

This work has been financially supported by the ANR (N°22-CE07-0024-*Evolution* Project). DA thanks the EUR LUMOMAT project and the Investments for the Future program ANR-18-EURE-0012 (PIPPIN) for a PhD grant. We also thank the CRMPO (Rennes) for mass analyses, the Inorganic Theoretical Chemistry (CTI) Team at ISCR and GENCI (Project N°AD010814136) for computing time. Dr Clement Brouillac and Dr Joelle Rault-Berthelot (Rennes) are acknowledged for their technical help in organic synthesis and electrochemistry respectively. Dr Olivier Jeannin (Rennes) is warmly thank for x-ray structure resolution.

Experimental Section

Experimental Details can be found in Supplementary Information.

References

[1]G. Hong, X. Gan, C. Leonhardt, Z. Zhang, J. Seibert, J. M. Busch, S. Bräse, *Adv. Mater.* **2021**, *33*, 2005630.

[2]M. A. Baldo, D. F. O'Brien, Y. You, A. Shoustikov, S. Sibley, M. E. Thompson, S. R. Forrest, *Nature* **1998**, *395*, 151-154.
[3]Y. Tao, C. Yang, J. Qin, *Chem. Soc. Rev.* **2011**, *40*, 2943-2970.
[4]K. S. Yook, J. Y. Lee, *Adv. Mater.* **2014**, *26*, 4218-4233.
[5]C. Poriel, J. Rault- Berthelot, *Adv. Funct. Mater.* **2021**, *31*, 2010547.
[6]C. Poriel, J. Rault-Berthelot, *Adv. Funct. Mat.* **2020**, *30*, 1910040.
[7]Y. Wang, J. H. Yun, L. Wang, J. Y. Lee, *Adv. Funct. Mater.* **2020**, *31*, 2008332.
[8]J.-H. Lee, C.-H. Chen, P.-H. Lee, H.-Y. Lin, M.-k. Leung, T.-L. Chiu, C.-F. Lin, *J. Mater. Chem. C* **2019**, *7*, 5874-5888.
[9]I. Siddiqui, S. Kumar, Y.-F. Tsai, P. Gautam, Shahnawaz, K. Kesavan, J.-T. Lin, L. Khai, K.-H. Chou, A. Choudhury, S. Grigalevicius, J.-H. Jou, *Nanomaterials* **2023**, *13*, 2521.
[10]C. Adachi, M. A. Baldo, M. E. Thompson, S. R. Forrest, *J. Appl. Phys.* **2001**, *90*, 5048-5051.
[11]M. A. Baldo, D. F. O'Brien, M. E. Thompson, S. R. Forrest, *Phys. Rev. B* **1999**, *60*, 14422-14448.
[12]H. Sasabe, J. Kido, *Eur. J. Org. Chem.* **2013**, 1653-1663.
[13]Q. Wang, Q.-S. Tian, Y.-L. Zhang, X. Tang, L.-S. Liao, *J. Mater. Chem. C* **2019**, *7*, 11329-11360.
[14]L. Xiao, Z. Chen, B. Qu, J. Luo, S. Kong, Q. Gong, J. Kido, *Adv. Mater.* **2011**, *23*, 926-952.
[15]K. S. Yook, J. Y. Lee, *Adv. Mater.* **2012**, *24*, 3169-3190.
[16]D. Y. Kondakov, W. C. Lenhart, W. F. Nichols, *J. Appl. Phys.* **2007**, *101*, 024512.
[17]N. Lin, J. Qiao, L. Duan, H. Li, L. Wang, Y. Qiu, *J. Phys. Chem. C* **2012**, *116*, 19451-19457.
[18]N. Lin, J. Qiao, L. Duan, L. Wang, Y. Qiu, *J. Phys. Chem. C* **2014**, *118*, 7569-7578.
[19]H. Li, M. Hong, A. Scarpaci, X. He, C. Risko, J. S. Sears, S. Barlow, P. Winget, S. R. Marder, D. Kim, J.-L. Brédas, *Chem. Mater.* **2019**, *31*, 1507-1519.
[20]S. Schmidbauer, A. Hohenleutner, B. König, *Adv. Mater.* **2013**, *25*, 2114-2129.
[21]K.-T. Wong, Y.-L. Liao, Y.-T. Lin, H.-C. Su, C.-C. Wu, *Org. Lett.* **2005**, *7*, 5131-5134.
[22]S. Ye, Y. Liu, C.-a. Di, H. Xi, W. Wu, Y. Wen, K. Lu, C. Du, Y. Liu, G. Yu, *Chem. Mater.* **2009**, *21*, 1333-1342.
[23]L.-C. Chi, W.-Y. Hung, H.-C. Chiu, K.-T. Wong, *Chem. Commun.* **2009**, 3892-3894.
[24]C. Fan, Y. Chen, P. Gan, C. Yang, C. Zhong, J. Qin, D. Ma, *Org. Lett.* **2010**, *12*, 5648-5651.
[25]M. Zhuo, W. Sun, G. Liu, J. Wang, L. Guo, C. Liu, B. Mi, J. Song, Z. Gao, *J. Mater. Chem. C* **2015**, *3*, 9137-9144.
[26]G. Tian, Y. Jiang, P. Wu, J. Huang, Q. Zou, Q. Wang, H. Mu, J. Su, *New J. Chem.* **2016**, *40*, 9500-9506
[27]X.-Y. Liu, X. Tang, Y. Zhao, D. Zhao, J. Fan, L.-S. Liao, *Dyes Pigm.* **2017**, *146*, 234-239.
[28]Y. Luo, Z. Liu, G. Yang, T. Wang, Z. Bin, J. Lan, D. Wu, J. You, *Angew. Chem. Int. Ed.* **2021**, *60*, 18852-18859.
[29]J. Ma, M. Idris, T. Y. Li, D. S. M. Ravinson, T. Fleetham, J. Kim, P. I. Djurovich, S. R. Forrest, M. E. Thompson, *Adv. Opt. Mater.* **2022**, *10*, 2101530.
[30]F. C. Kong, Y. L. Zhang, C. Quinton, N. McIntosh, S. Y. Yang, J. Rault-Berthelot, F. Lucas, C. Brouillac, O. Jeannin, J. Cornil, Z. Q. Jiang, L. S. Liao, C. Poriel, *Angew Chem Int Ed Engl* **2022**, *61*, e202207204.
[31]A. Yoshii, Y. Onaka, K. Ikemoto, T. Izumi, S. Sato, H. Kita, H. Taka, H. Isobe, *Chem. Asian J.* **2020**, *15*, 2181-2186.
[32]J. Y. Xue, T. Izumi, A. Yoshii, K. Ikemoto, T. Koretsune, R. Akashi, R. Arita, H. Taka, H. Kita, S. Sato, H. Isobe, *Chem. Sci.* **2016**, *7*, 896-904.
[33]K. Ikemoto, A. Yoshii, T. Izumi, H. Taka, H. Kita, J. Y. Xue, R. Kobayashi, S. Sato, H. Isobe, *J. Org. Chem.* **2016**, *81*, 662-666.
[34]C. Poriel, J. Rault-Berthelot, *Acc. Mater. Res.* **2022**, *3*, 379-390.
[35]C. Poriel, J. Rault-Berthelot, Z.-Q. Jiang, *Mater. Chem. Front.* **2022**, *6*, 1246-1252.
[36]C. Poriel, C. Quinton, F. Lucas, J. Rault- Berthelot, Z. Q. Jiang, O. Jeannin, *Adv. Funct. Mater.* **2021**, 2104980.
[37]J.-D. Peltier, B. Heinrich, B. Donnio, O. A. Ibraikulov, T. Heiser, N. Leclerc, J. Rault-Berthelot, C. Poriel, *Mater. Chem. Front.* **2022**, *6*, 225-236.
[38]C. Brouillac, F.-C. Kong, J. Rault-Berthelot, C. Quinton, Z.-Q. Jiang, C. Poriel, *Adv. Mater. Technol.* **2023**, *n/a*, 2300763.
[39]J.-D. Peltier, B. Heinrich, B. Donnio, O. Jeannin, J. Rault-Berthelot, E. Jacques, C. Poriel, *J. Mater.*

Chem. C **2018**, *6*, 13197-13210.
[40]T. P. I. Saragi, T. Spehr, A. Siebert, T. Fuhrmann-Lieker, J. Salbeck, *Chem. Rev.* **2007**, *107*, 1011-1065.
[41]T. Fuhrmann, J. Salbeck, *Adv. Photochem.* **2002**, *27*, 83-166.
[42]C. Poriel, L. Sicard, J. Rault-Berthelot, *Chem. Comm.* **2019**, *55*, 14238-14254.
[43]S. Liu, D. Xia, M. Baumgarten, *ChemPlusChem* **2021**, *21*, 36-48.
[44]Y. Chen, J. Xu, P. Gao, *Org. Chem. Front.* **2024**.
[45]C. Quinton, S. Thiery, O. Jeannin, D. Tondelier, B. Geffroy, E. Jacques, J. Rault-Berthelot, C. Poriel, *ACS Appl. Mater. Interfaces.* **2017**, *9*, 6194–6206.
[46]S. Thiery, C. Declairieux, D. Tondelier, G. Seo, B. Geffroy, O. Jeannin, R. Métivier, J. Rault-Berthelot, C. Poriel, *Tetrahedron* **2014**, *70*, 6337-6351.
[47]D. Thirion, C. Poriel, F. Barrière, R. Métivier, O. Jeannin, J. Rault-Berthelot, *Org. Lett.* **2009**, *11*, 4794-4797.
[48]V. J. Chebny, R. Shukla, S. V. Lindeman, R. Rathore, *Org. Lett.* **2009**, *11*, 1939-1942.
[49]R. Rathore, S. H. Abdelwahed, I. A. Guzei, *J. Am. Chem. Soc.* **2003**, *125*, 8712-8713.
[50]L. Sicard, C. Quinton, F. Lucas, O. Jeannin, J. Rault-Berthelot, C. Poriel, *J. Phys. Chem. C* **2019**, *123*, 19094-19104.
[51]L. Sicard, C. Brouillac, N. Leclerc, S. Fall, N. Zimmerman, O. Jeannin, J. Rault-Berthelot, C. Quinton, C. Poriel, *Mater. Chem. Front.* **2024**, *8*, 1349-1361.
[52]C. Poriel, J. Rault-Berthelot, F. Barrière, A. M. Z. Slawin, *Org. Lett.* **2008**, *10*, 373-376.
[53]L. J. Sicard, H.-C. Li, Q. Wang, X.-Y. Liu, O. Jeannin, J. Rault-Berthelot, L.-S. Liao, Z.-Q. Jiang, C. Poriel, *Angew. Chem. Int. Ed.* **2019**, *58*, 3848-3853.
[54]L.-S. Cui, Y.-M. Xie, Y.-K. Wang, C. Zhong, Y.-L. Deng, X.-Y. Liu, Z.-Q. Jiang, L.-S. Liao, *Adv. Mater.* **2015**, *27*, 4213-4217.
[55]F. Lucas, C. Quinton, S. Fall, T. Heiser, D. Tondelier, B. Geffroy, N. Leclerc, J. Rault-Berthelot, C. Poriel, *J. Mater. Chem. C* **2020**, *8*, 16354-16367.
[56]F. Lucas, C. Brouillac, S. Fall, N. Zimmerman, D. Tondelier, B. Geffroy, N. Leclerc, T. Heiser, C. Lebreton, E. Jacques, C. Quinton, J. Rault-Berthelot, C. Poriel, *Chem. Mater.* **2022**, *34*, 8345–8355.
[57]E. Baranoff, B. F. E. Curchod, *Dalton Trans.* **2015**, *44*, 8318-8329.
[58]J. Jayabharathi, V. Thanikachalam, S. Thilagavathy, *Coord. Chem. Rev.* **2023**, *483*, 215100.